Momentum peak shift and width of longitudinal momentum distribution of projectilelike fragments produced at $E = 290$ MeV/nucleon

S. Momota,[1,*] M. Kanazawa,[2] A. Kitagawa,[3] and S. Sato[3]

[1]*Kochi University of Technology, Kochi 782-8502, Japan*

[2]*SAGA Heavy Ion Medical Accelerator in Tosu, Tosu, Saga 841-0071, Japan*

[3]*National Institute of Radiological Sciences, National Institutes for Quantum and Radiological Science and Technology, Chiba 263-8555, Japan*

(Received 27 October 2017; revised manuscript received 27 January 2018; published 11 April 2018)

Longitudinal momentum (P_L) distributions of projectilelike fragments produced at $E = 290$ MeV/nucleon are investigated. P_L distributions of fragments produced by Ar and Kr beams with a wide variety of targets (C, Al, Nb, Tb, and Au) were measured using the fragment separator at HIMAC. P_L distributions observed for fragments with a wide range of mass losses ΔA (1–30 for Ar beam and 1–64 for Kr beam), show a slightly, but definitely asymmetric nature. The peak shift and width were obtained from the observed P_L distributions. No significant target dependence was found in either the peak shift or width. For the practical application, the variation in momentum peak shift with fragment mass (A_F) was represented by a parabolic function. The width on the high-P_L side (σ_{High}) is well reproduced by the Goldhaber formula, which is obtained from the contribution of the Fermi momentum. The behavior of the reduced width, σ_0, obtained from σ_{High} via the Goldhaber formulation, is consistent with the mass-dependent Fermi momentum of a nucleon. The width on the low-P_L side (σ_{Low}) is markedly larger than σ_{High} and exhibits a clear A_F dependence.

DOI: 10.1103/PhysRevC.97.044604

I. INTRODUCTION

Fragmentation reactions of projectiles with intermediate or relativistic energies play an important role in the production and investigation of unstable nuclei, far from the valley of β stability. Systematic information on the momentum distribution of fragments is crucial for designing experiments with produced fragments. A series of experimental and theoretical studies have been carried out to reveal the momentum distribution of fragments. The systematics or parameterized formulas of momentum distribution is incorporated within programs, such as LISE++ [1] and MOCADI [2], which enable the intensities and purities of fragments to be determined. In general, the momentum distributions of fragmentation products are well reproduced by a Gaussian with a narrow width [3]. The characteristics of the distribution can be represented by two indices: (i) width and (ii) peak shift from the peak corresponding to the projectiles. These indices are also important factors for investigating the mechanism of the fragmentation process.

At relativistic energies ($E > 1$ GeV/nucleon), the distribution becomes isotropic and its width has been successfully predicted by simple models proposed by Goldhaber [4] and Morrissey [5]. According to the Goldhaber model, the width of the momentum distribution is understood on the basis of the Fermi momentum of removed nucleons, and formulated in terms of the mass numbers of the projectile, A_P, and of the fragment, A_F, and the reduced width, σ_0. A number of experimental studies have shown that the value of σ_0 fluctuates around 100 MeV/c depending on the reaction parameter. The behavior of σ_0 was investigated and formulated as a function of A_P and the incident energy in Refs. [6–9]. At lower energies ($E < 100$ MeV/nucleon), momentum distributions exhibit anisotropic features. For the longitudinal momentum (P_L), a larger width or a tail component has been observed on the low-P_L side [10–12]. In order to explain the additional width, the contribution of energy-dissipative processes, such as the nucleon-exchange reaction, was considered in Ref. [12]. The scarcity of experimental results, especially at intermediate energies ($E = 100$–500 MeV/nucleon), prevents us from validating the formulas for σ_0 and determining the contribution of energy-dissipative processes.

The P_L distribution of fragments also shows a small but significant momentum shift from the P_L corresponding to projectiles. The momentum shift, which is due to the momentum transfer through fragmentation, exhibits a clear A_F dependence and was investigated at relativistic and lower energies in Refs. [3,5,13] and [11,12], respectively. In Ref. [14], an *N/Z*-dependent momentum peak shift was observed at 500 MeV/nucleon.

In the present study, the P_L distribution of fragments produced through fragmentation process at $E = 290$ MeV/nucleon was investigated. Fragments produced by Ar and Kr beams and targets with a wide range of masses were observed. Parts of these experimental results have been reported in our previous paper [15]. However, the analysis of the observed P_L distributions was insufficient. In the present paper, all of the observed P_L distributions are analyzed to obtain the momentum peak shift and the width of the P_L distribution. The systematic behavior of the peak shift and the

*Corresponding author: momota.sadao@kochi-tech.ac.jp

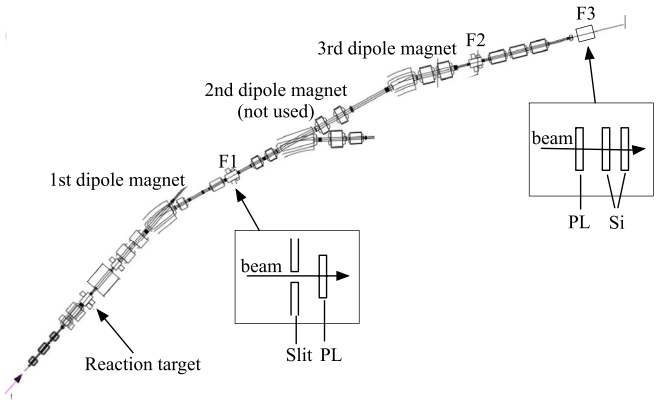

FIG. 1. Schematic of secondary beam course SB2.

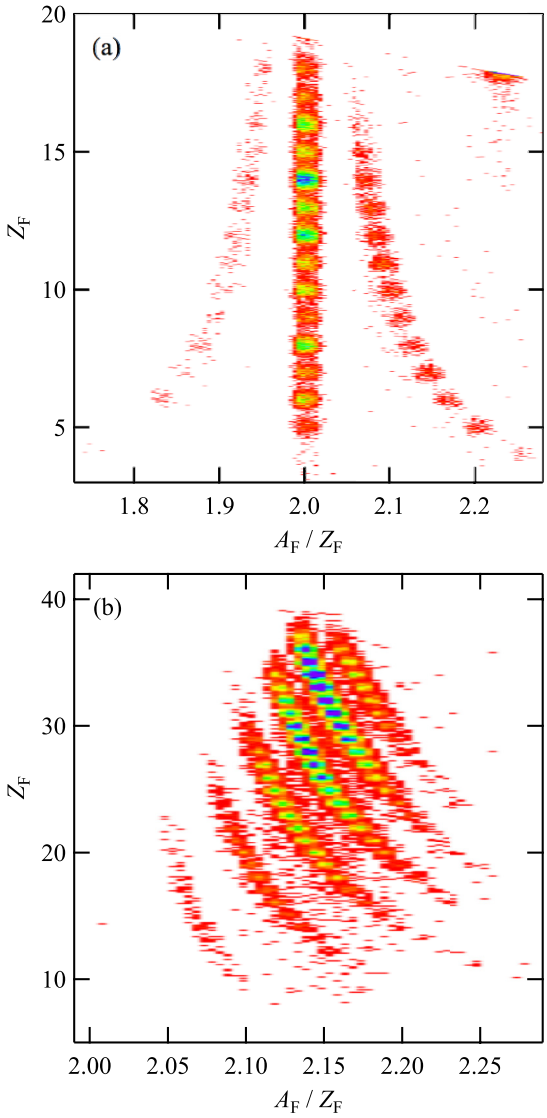

FIG. 2. Particle identification of fragments produced by reactions with (a) an Ar beam and Tb target at $B\rho = 5.088$ Tm, and (b) a Kr beam and Tb target at $B\rho = 5.462$ Tm.

TABLE I. Energy loss and straggling of projectile in reaction targets

Incident beam	Target	Energy loss (MeV/nucleon)	Energy straggling[a] (MeV/nucleon)	Angular straggling[a] (mrad)
^{40}Ar	C	5.13	0.07	0.60
	Al	4.80	0.07	0.82
	Nb	8.33	0.10	1.87
	Tb	5.95	0.09	1.96
	Au	10.06	0.11	2.82
^{84}Kr	C	9.90	0.07	0.57
	Al	9.26	0.07	0.79
	Nb	16.18	0.09	1.81
	Tb	11.57	0.09	1.89
	Au	19.62	0.12	2.72

[a]Energy and angular straggling represents one standard deviation.

TABLE II. Momentum and angular acceptance of SB2.

Incident beam	$\Delta P/P$[a] (%)	$\Delta\theta_x$[b] (mrad)	$\Delta\theta_y$[b] (mrad)
^{40}Ar	1	±13	±13
^{84}Kr	0.5	±13	±13

[a]Momentum acceptance represents that corresponds to the slits at F1.
[b]Angular acceptance represents that corresponds to the four slits behind the reaction target. The four slits were used to define the angular acceptance with a square shape in the θ_x-θ_y plane.

TABLE III. Resolution of TOF spectrum for primary beam.

	Resolution (nsec)[a]	
Target	Ar beam	Kr beam
C	-[b]	0.07
Al	-[b]	0.05
Nb	0.06	0.07
Tb	0.11	0.07
Au	0.11	0.06

[a]Resolution of TOF represents one standard deviation.
[b]Time of flight spectrum for primary beam was not observed.

TABLE IV. Fitting results for momentum peak shift, ΔP_L.

Target	a (MeV/c)	b	c (MeV/c)
Ar beam			
C	0.70 ± 0.11	17.81 ± 1.29	–289.4 ± 10.1
Al	0.77 ± 0.13	21.33 ± 0.98	–266.4 ± 8.7
Nb	0.75 ± 0.15	21.55 ± 1.02	–268.9 ± 13.2
Tb	0.68 ± 0.08	21.19 ± 0.57	–258.8 ± 7.0
Au	0.71 ± 0.10	20.18 ± 0.86	–276.8 ± 7.7
Kr beam			
C	0.51 ± 0.02	48.79 ± 0.49	–628.1 ± 10.4
Al	0.52 ± 0.02	50.13 ± 0.36	–600.5 ± 9.8
Nb	0.56 ± 0.03	50.57 ± 0.55	–619.4 ± 7.1
Tb	0.47 ± 0.02	49.65 ± 0.44	–601.7 ± 7.1
Au	0.54 ± 0.01	50.19 ± 0.23	–640.7 ± 6.3

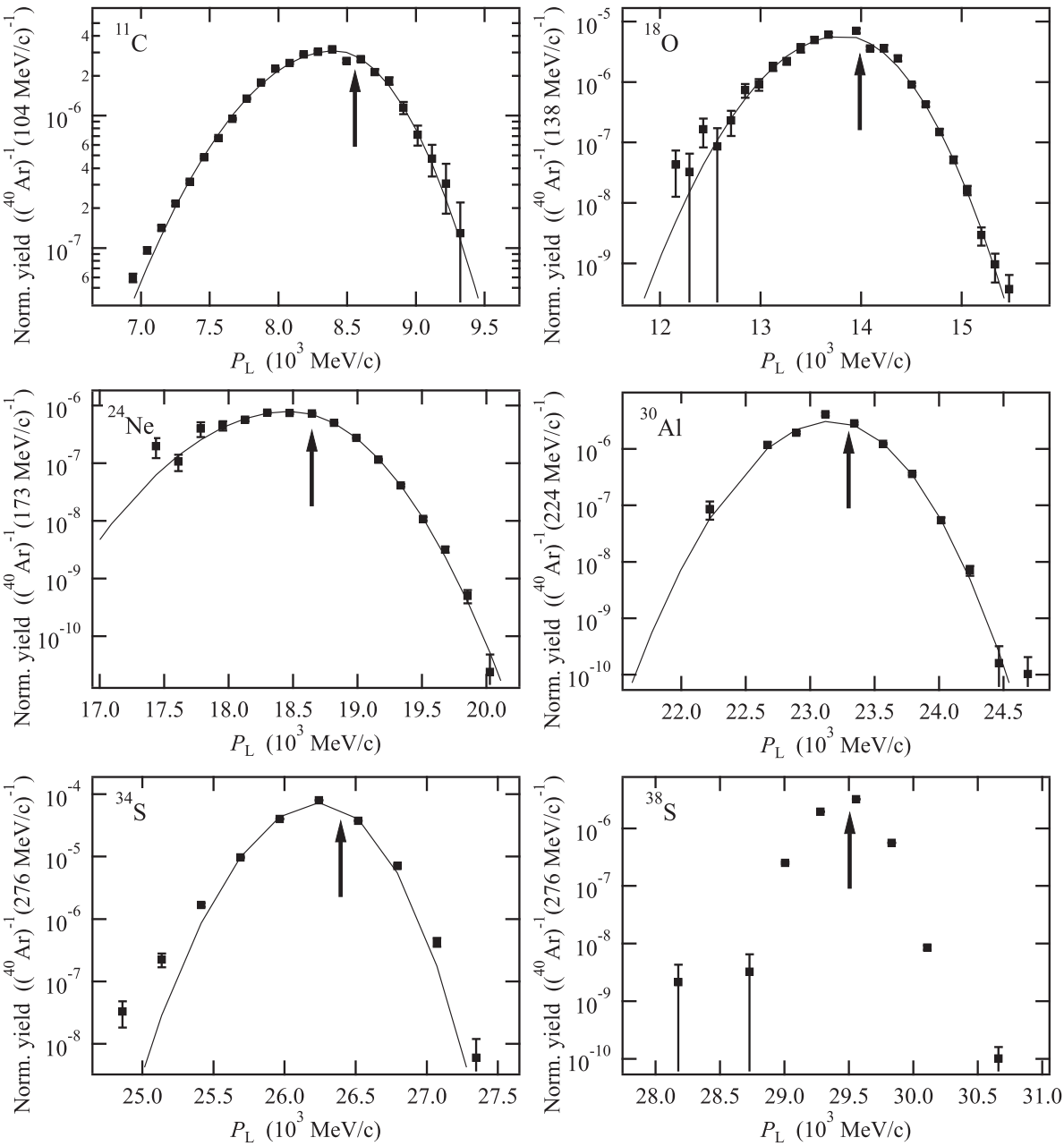

FIG. 3. P_L distributions of fragments produced by Ar beam and Nb target. Arrows indicate momentum of each fragment corresponding to velocity of projectile, ^{40}Ar, after Nb target. Solid curves represent fits to the asymmetric Gaussian function in Eq. (1).

width will be discussed and formulated for practical use. By combining with results obtained in other experimental studies, the validity of the formulas for σ_0 will be confirmed.

II. EXPERIMENT

The experiment was performed at the National Institute of Radiological Sciences (NIRS). ^{40}Ar and ^{84}Kr beams were accelerated up to 290 MeV/nucleon by the HIMAC accelerator and irradiated onto targets with a wide range of masses (C, Al, Nb, Tb, and Au). The thicknesses of the C, Al, Nb, Tb, and Au targets were 195, 206, 440, 362, and 643 mg/cm^2, respectively. Table I summarizes the energy loss and stragglings of the incident beams in those targets, which were calculated using the ATIMA code [16].

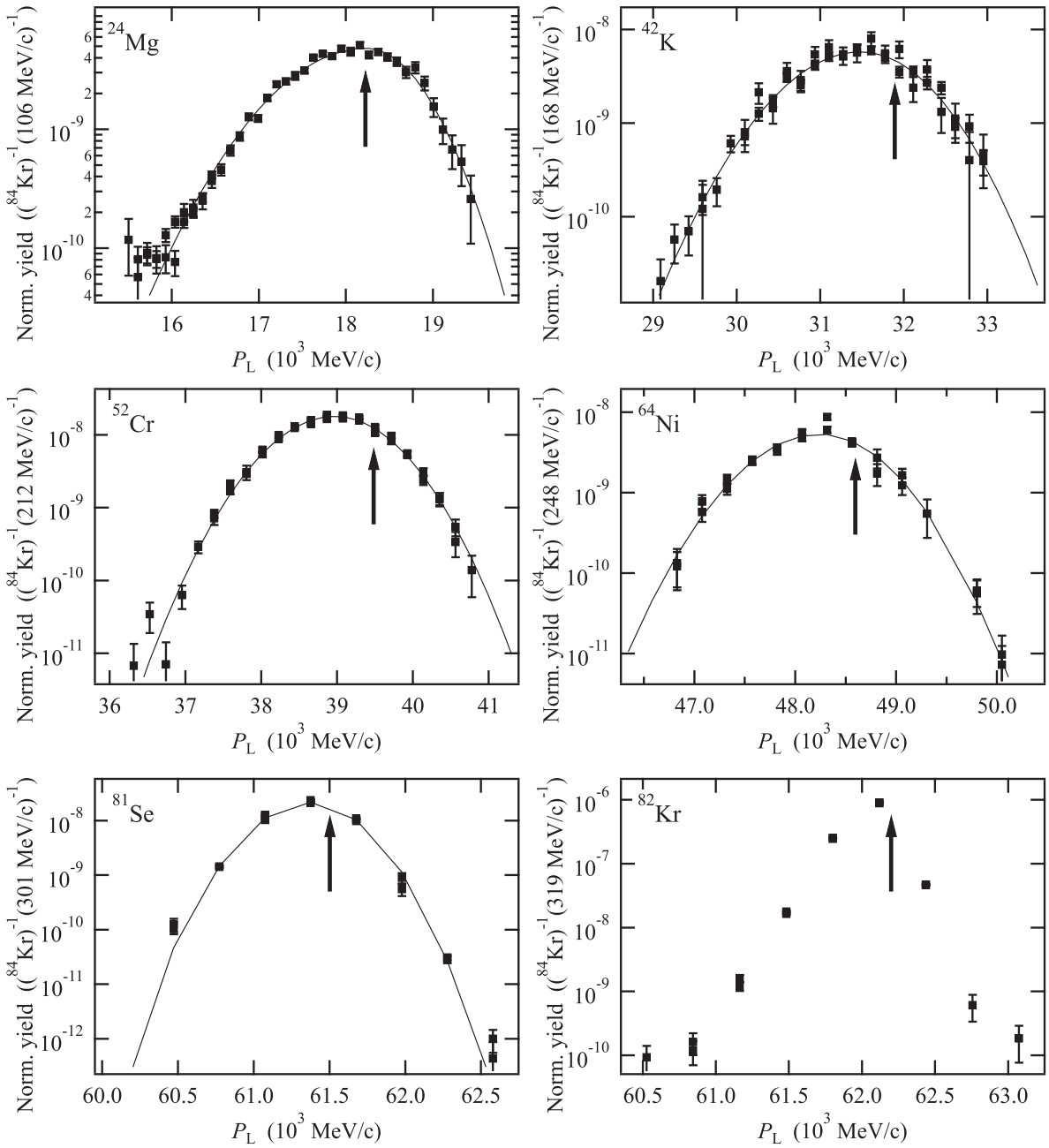

FIG. 4. P_L distributions of fragments produced by Kr beam and Au target. Arrows and solid curves as described in Fig. 3.

The high-energy beam transport system SB2 [17], shown in Fig. 1, was applied as a spectrometer to identify the reaction products. The reaction products were collected and transported to a doubly achromatic focal plane F3, where the momentum dispersion function and its derivative along the beam line are both zero. The momentum acceptance of the spectrometer was defined at the momentum dispersive focusing point F1, and the angular acceptance was defined with a square window formed by four slits (upper, lower, left, and right), which were located 3 m behind the reaction target. The momentum and angular acceptances applied for each incident beam were fixed to the values tabulated in Table II. Fragment identification was conducted on an event-by-event basis through time-of-flight (TOF) and energy loss (ΔE) measurements, which are almost identical to those reported in our previous paper [18]. In principle, two plastic scintillation counters (PL's), installed at F1 and F3, were used to measure the TOF, and ΔE of the fragment was measured with a silicon (Si) counter installed at F3. In the measurements with Ar beam and C target, PL's, installed at F1 and F2, and a Si counter installed at F2 were used. The time resolutions of TOF, measured with the primary beam, are summarized in Table III. The P_L distribution was observed by changing stepwise the rigidity of the SB2 spectrometer, $B\rho$. According to the charge-state distribution

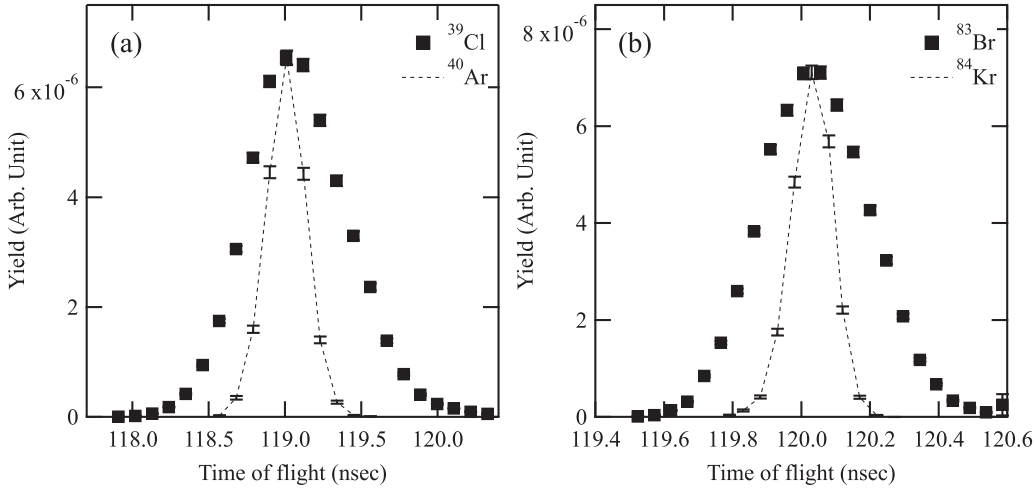

FIG. 5. TOF distributions of fragments produced through reactions of (a) ^{40}Ar + ^{159}Tb and (b) ^{84}Kr + ^{159}Tb. Dotted curves represent TOF distributions for projectile. For comparison, the amplitude and peak value for projectile are adjusted to those for fragments.

of the reaction products at 290 MeV/nucleon, which was evaluated using the CHARGE code [19], the contributions of products that were not fully stripped were approximately 2% or less. The mass number, A_F, and atomic number, Z_F, of the fragment were obtained from the observed TOF, ΔE, and $B\rho$. The fragment yields were obtained by counting the isotopes using the described identification method.

The primary beam intensity was monitored for normalization of the fragment yields to obtain the P_L distribution of the fragmentation products. The beam intensity was measured as the count of electrons emitted from a thin foil inserted in the beam line upstream from the target. For every measurement, the count rate of emitted electrons was calibrated using a parallel-plate ionization chamber. Calibration data were acquired by changing the primary beam intensity, which ranged from 10^{-3} to 1.0 times the maximum beam intensity. The relative error in the primary beam intensity due to the uncertainty in the calibration was approximately ±5%.

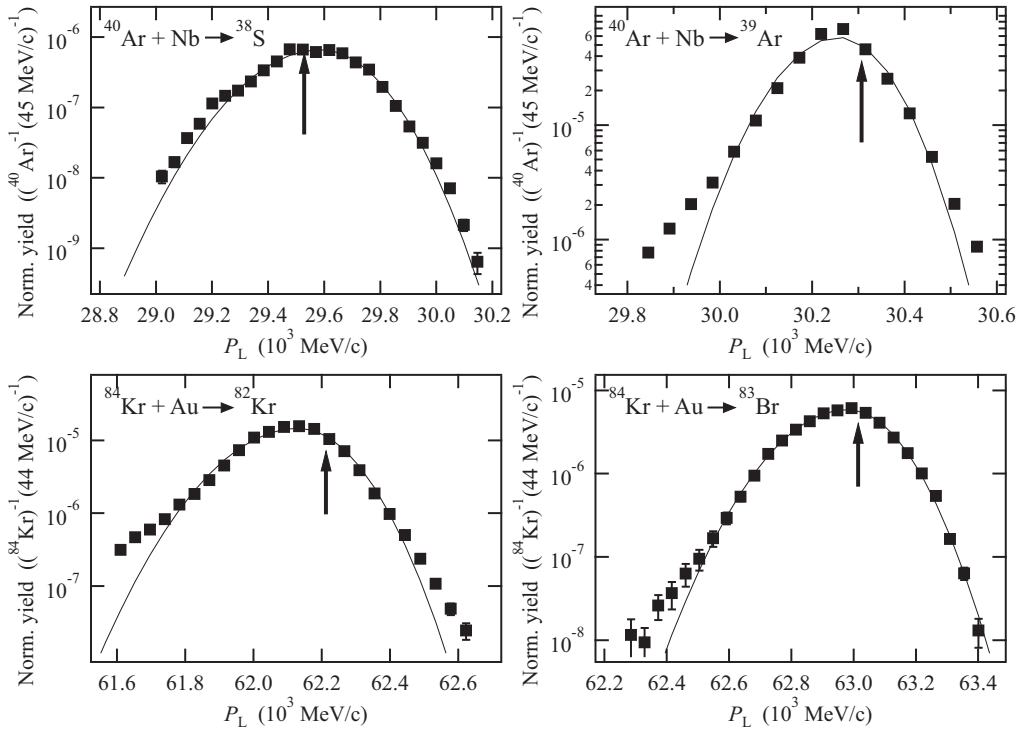

FIG. 6. P_L distributions of fragments produced through few-nucleon removal reactions. The distributions were obtained from TOF data. Arrows and curves as described in Fig. 3.

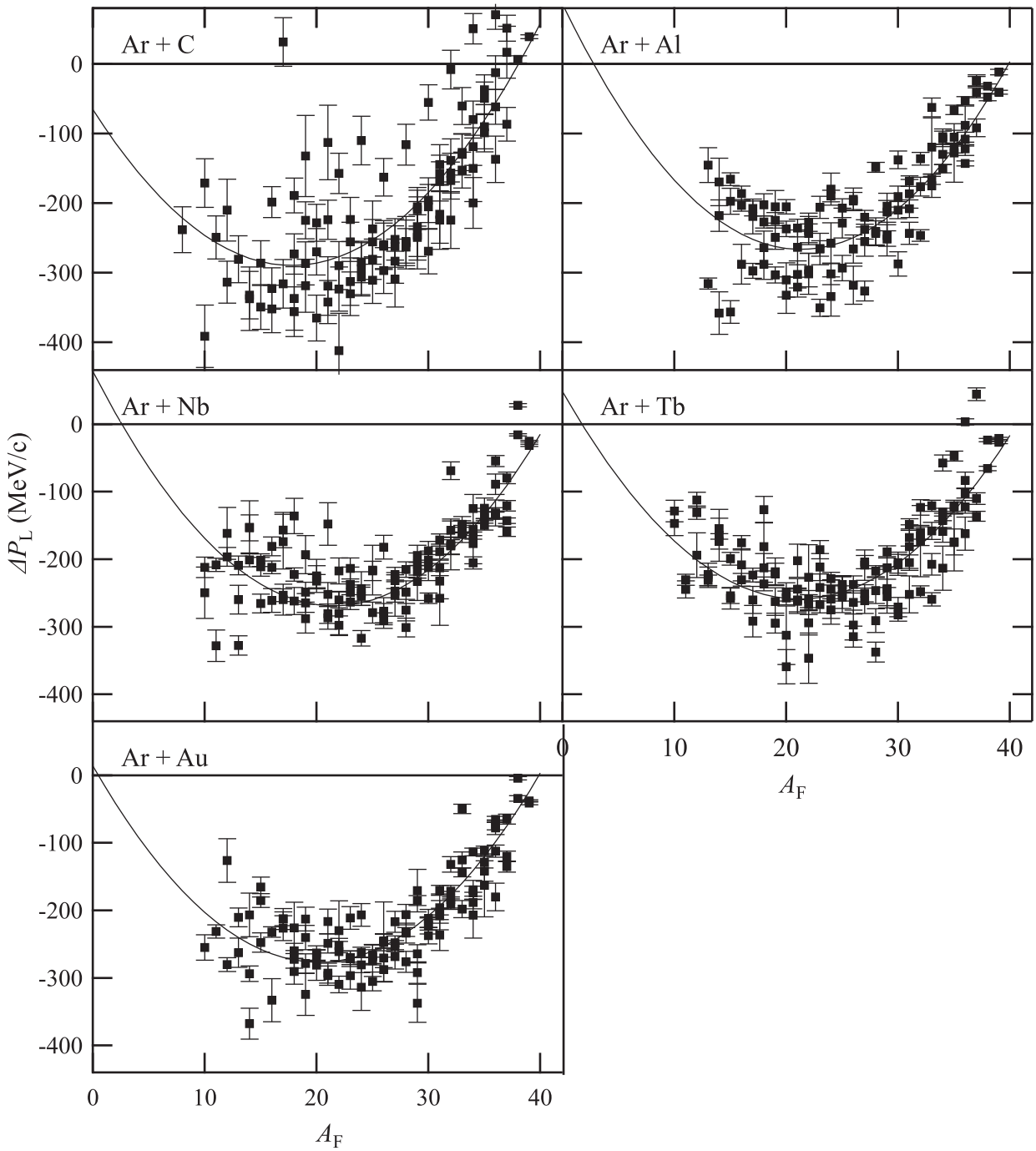

FIG. 7. Momentum shift of fragments produced by Ar beam. Solid lines represent a fit to Eq. (3).

III. RESULTS AND DISCUSSION

A. Particle identification and counting of fragmentation products

Figure 2 shows the typical Z versus A/Z plots obtained in this study. The A/Z values are well resolved, owing to the sufficiently narrow momentum acceptance and high resolution of the TOF measurement. As described in Ref. [18], the ambiguity of counting for each fragment, which was determined from the degree of contamination, was found to be approximately 1% (10%) for the Ar (Kr) beam by analyzing the Z-projection spectrum. The measured yield was normalized by the primary beam intensity. The transmission between the target to F3 was not determined and the transmission value is assumed to be constant for every individual fragment. The error in the normalized yield of the observed fragments is evaluated based on three contributions: statistical error, uncertainty in calibration of beam intensity, and ambiguity in counting.

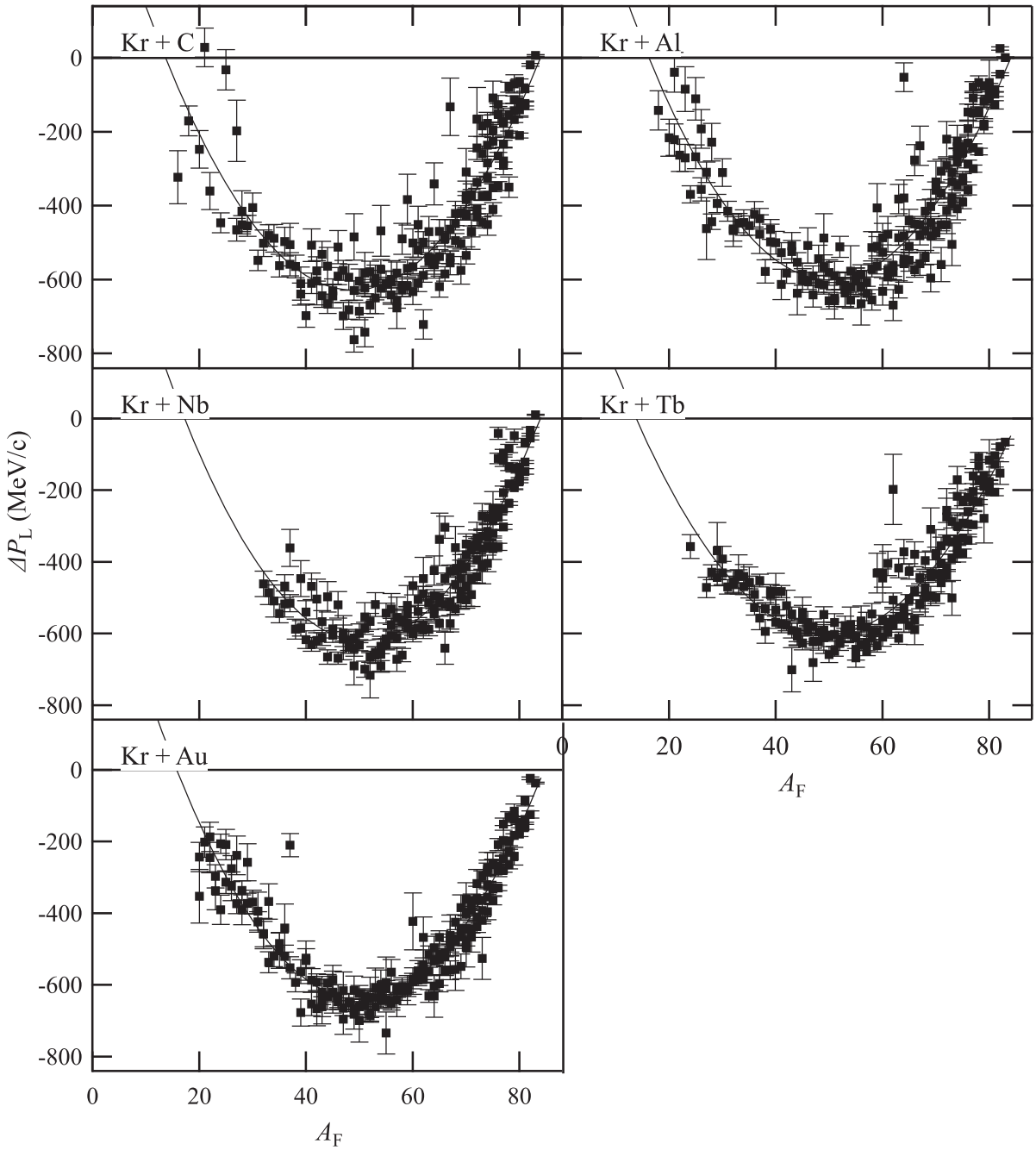

FIG. 8. Momentum peak shift of fragments produced by Kr beam. Solid lines represent a fit to Eq. (3).

B. Analysis of observed P_L distributions

Figures 3 and 4 show the observed P_L distributions of fragments with an Ar and Kr beam, respectively. P_L was calculated from Z_F and A_F, which are obtained from particle identification, and the $B\rho$ of the SB2 spectrometer. The contribution of limited angular acceptance (see Table II) is corrected on the basis of the transverse momentum distributions, as proposed by Goldhaber [4] and Van Bibber *et al.* [20]. As shown in the figures, measurements of P_L distribution were made successfully over a wide A_F range. The ranges of A_F/Z_F values for the observed fragments were 1.8–2.6 and 2.0–2.4 for the Ar beam and Kr beam, respectively. The figures show a small momentum peak shift toward the low-P_L side and a larger width on the low-P_L side, observed at $E \approx 100$ MeV/nucleon [12]. In the case of the few-nucleons removal reaction, a step of P_L, which is determined by a step of the $B\rho$ setting, is comparable or larger than the width of the P_L distribution and it is difficult to conduct a valid analysis. In contrast, the TOF distribution shows a clearly defined shape and is thus suited for analysis, as shown in Fig. 5. In order to obtain reliable values for the momentum peak shift and the width for the fragments, which are produced by a one- or two-nucleons

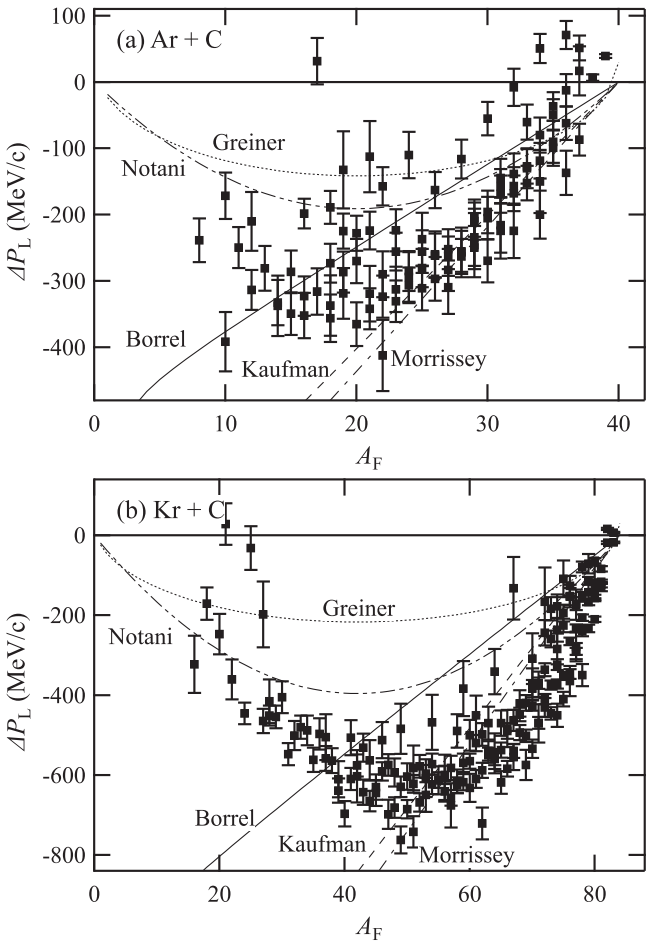

FIG. 9. Momentum peak shift of fragments compared with formulation.

removal reaction, the P_L distribution is obtained from the TOF data, as shown in Fig. 6.

The observed P_L distributions are analyzed by using the following function [12]:

$$Y(p) = \begin{cases} k \exp\left(-\frac{(p-p_0)^2}{2\sigma_{\mathrm{Low}}{}^2}\right) & \text{for} \quad p \leqslant p_0 \\ k \exp\left(-\frac{(p-p_0)^2}{2\sigma_{\mathrm{High}}{}^2}\right) & \text{for} \quad p > p_0, \end{cases} \tag{1}$$

where k is the normalization factor, p_0 is the peak value of P_L, σ_{Low} and σ_{High} are the widths on the low- and high-P_L sides. The contribution of the finite P_L bin, as defined by the acceptance of the SB2 separator or TOF, is considered in the fitting process. The fitting results with Eq. (1) well reproduce the experimental results as indicated by the solid curves in Figs. 3, 4, and 6. The energy loss in the reaction target, which depends on the fragment and the reaction position, induces a change in the peak value and an additional peak width from the values determined intrinsically by the fragmentation process. In order to correct the contribution of the change in the peak value, $p_0{}'$, which corresponds to the peak value of P_L at the center of the reaction target, is determined from p_0 and will be used in the following analysis. The contribution of the additional peak width was subtracted from the widths σ_{Low} and σ_{High}, obtained by the fitting. As shown in Fig. 5, the effect of the TOF resolution is not negligible for fragments that are produced by a one- and also two-nucleons removal reaction. For those fragments other than those produced from the reactions Ar+C and Ar+Al, the contribution due to the TOF resolution was also subtracted.

TABLE V. Reduced width of P_L distributions, σ_0.

Target	σ_0 (MeV/c) High-P_L	σ_0 (MeV/c) Low-P_L	Low-P_L / High-P_L
Ar beam			
C	104.1 ± 3.1	153.9 ± 3.4	1.48 ± 0.05
Al	110.5 ± 2.8	165.1 ± 4.7	1.49 ± 0.06
Nb	106.8 ± 3.2	136.8 ± 2.4	1.28 ± 0.04
Tb	106.3 ± 2.9	138.3 ± 3.0	1.30 ± 0.05
Au	104.1 ± 2.9	138.7 ± 3.0	1.33 ± 0.05
Kr beam			
C	117.5 ± 2.7	152.4 ± 3.5	1.30 ± 0.04
Al	113.0 ± 2.8	150.0 ± 2.9	1.33 ± 0.04
Nb	110.8 ± 2.8	141.1 ± 2.9	1.27 ± 0.04
Tb	115.0 ± 3.1	145.1 ± 3.3	1.26 ± 0.05
Au	113.5 ± 2.5	141.6 ± 2.8	1.25 ± 0.04
^{40}Ca beam, 141 MeV/nucleon[a]			
Be	85 ± 8	125 ± 10	1.47 ± 0.18
Ta	84 ± 7	117 ± 9	1.39 ± 0.16
^{86}Kr beam, 66 MeV/nucleon[a]			
Be	121 ± 8	175 ± 11	1.45 ± 0.13
Ta	119 ± 10	181 ± 9	1.52 ± 0.15

Errors are calculated from standard deviation for each reaction.
[a]Values of σ_0 are from Table 4.1 in Ref. [21].

C. Momentum peak shift of fragmentation products

Figures 7 and 8 show the momentum peak shift, ΔP_L, as a function of A_F, produced by Ar and Kr beams, respectively. ΔP_L is defined as

$$\Delta P_L = p_0{}' - p_P, \tag{2}$$

where p_P is the P_L of the fragment corresponding to the projectile velocity at the center of the reaction target. Systematic decelerative properties, obtained with Ar and Kr beams [12,21,22], are clearly observed. In principle, the observed A_F dependence shows a paraboliclike shape and no significant target dependence. In order to confirm the validity of the previously proposed formulas, ΔP_L calculated by the formulas is shown with the present results in Fig. 9. The formulas by Greiner [3] and Notani [12], which show a parabolic shape, underestimate the decelerative nature of the ΔP_L. The formulas by Morrissey [5] and Kaufman [13] give reasonable values for fragments with A_F values between $A_P/2$ and A_P, however, fail to represent the parabolic shape.

For practical use, the present results are analyzed using a parabolic function:

$$\Delta P_L = a(A_F - b)^2 - c. \tag{3}$$

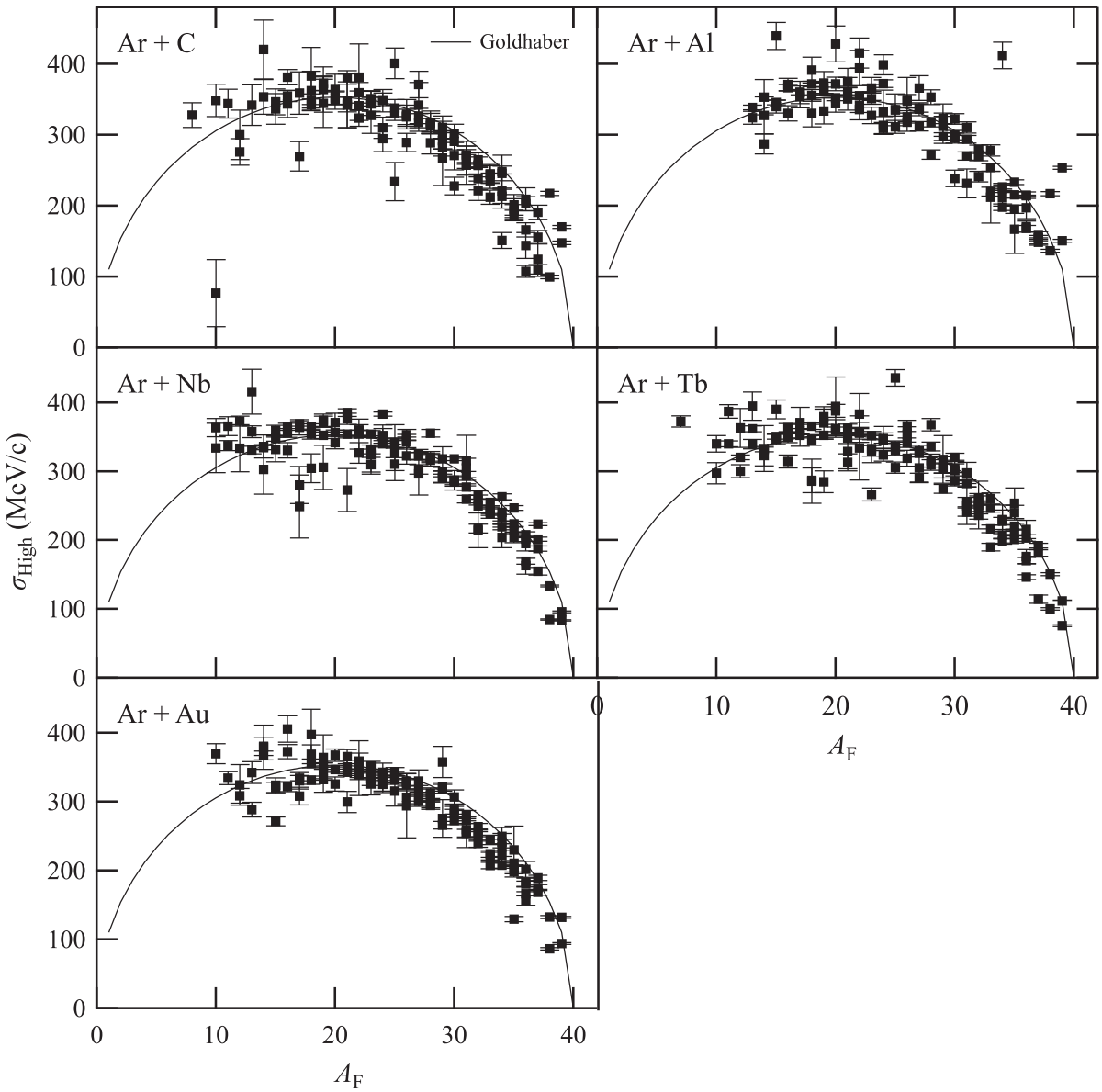

FIG. 10. Width of $P_{\rm L}$ distribution obtained on the high-$P_{\rm L}$ side with Ar beam. Solid lines show the formulation proposed in Goldhaber [4] with reduced width, $\sigma_0 = 110.2\,{\rm MeV}/c$ [9].

The fitting results are indicated by solid lines in Figs. 7 and 8 and tabulated in Table IV.

D. Width of observed $P_{\rm L}$ distributions

The width on the high-$P_{\rm L}$ side, $\sigma_{\rm High}$, is shown as a function of $A_{\rm F}$ in Figs. 10 and 11. As with $\Delta P_{\rm L}$, no significant target dependence is observed. The paraboliclike shape suggests the validity of the Goldhaber formulation [4]. $\sigma_{\rm High}$, observed with a C target, is shown in Fig. 12 with the width calculated by the formulas proposed in Refs. [4,5,23]. All relevant processes are included as an analytical formulation in Ref. [23]. The Morrissey formulation [5] is valid for fragments with relatively small mass losses. In all of the observed $A_{\rm F}$ regions, the formulas proposed in Refs. [4] and [23] give consistent results.

According to Ref. [4], the $P_{\rm L}$ distribution is formulated with a reduced width, σ_0, and σ_0 is obtained from the Fermi momentum of nucleons, $p_{\rm F}$, via the following relationship:

$$\sigma_0 = \frac{p_{\rm F}}{\sqrt{5}}. \tag{4}$$

σ_0, calculated from the observed $\sigma_{\rm High}$ by the formula in Ref. [4], is shown as a function of $A_{\rm F}$ in Figs. 13 and 14. The arithmetic means of σ_0 in the observed $A_{\rm F}$ range are indicated by broken lines in those figures and tabulated in Table V. Previous investigations into the $P_{\rm L}$ distribution of fragments have shown that σ_0 fluctuates depending on the reaction parameters, such as energy of projectile, E, and $A_{\rm P}$. The E dependence of σ_0 for Ar and Kr beams is shown in Fig. 15. The observed σ_0 shows no significant energy

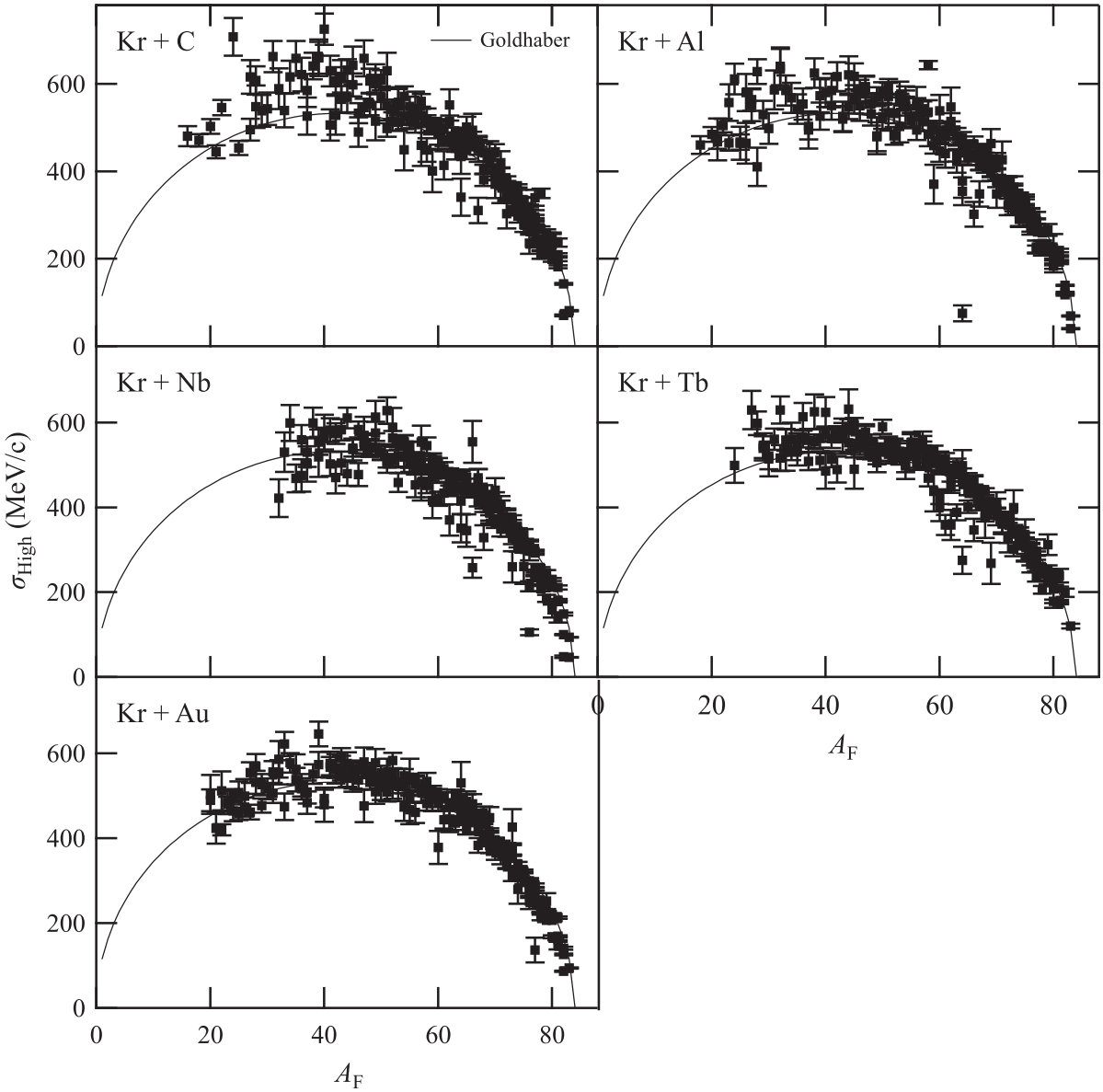

FIG. 11. Width of P_{L} distribution obtained on the high-P_{L} side with Kr beam. Solid lines as described in Fig. 10. $\sigma_0 = 115.5\,\mathrm{MeV}/c$ [9] is used for calculation.

dependence. The absolute value of σ_0 and its behavior is well reproduced by a best-fit approximation to the measured values presented in Ref. [9], which is based on the mass number dependence of p_{F}. On the other hand, the parameterization presented in Ref. [6] is inconsistent, especially for the Kr beam. The A_{P} dependence of σ_0, which was observed at $E > 100$ MeV/nucleon, is shown in Fig. 16. Excluding a few results observed with a Kr beam [14,22], the behavior of the observed σ_0, which shows a monotonic increase with A_{P}, is roughly reproduced by the formula in Ref. [9].

The width on the low-P_{L} side, σ_{Low}, is shown as a function of A_{F} in Figs. 17 and 18. σ_{Low} shows no significant target dependence, as in the case of σ_{High}, and is significantly larger than σ_{High}, as observed at lower energy. These results confirm the contribution of additional reaction processes, such as the nucleon-exchange reaction, whose significance, however, is suppressed compared to that at lower energy. In Ref. [12], σ_{Low} converges to 300–400 MeV/c as the mass change $\Delta A \to 0$. This indicates that additional reaction processes maintain a meaningful contribution even in the small-ΔA reaction at $E \approx 100$ MeV/nucleon. In contrast, σ_{Low} converges to 0 as $\Delta A \to 0$ in the present study. This implies that the contribution of additional reaction processes is suppressed in the small-ΔA reaction at $E = 290$ MeV/nucleon. σ_0, obtained from σ_{Low}, and its ratio to that obtained from σ_{High} are summarized in Table V. According to these results, σ_{Low} is about 30–50% larger than σ_{High}. As shown with broken lines in Figs. 17 and 18, this relationship is valid for fragments with $A_{\mathrm{F}} > A_{\mathrm{P}}/2$.

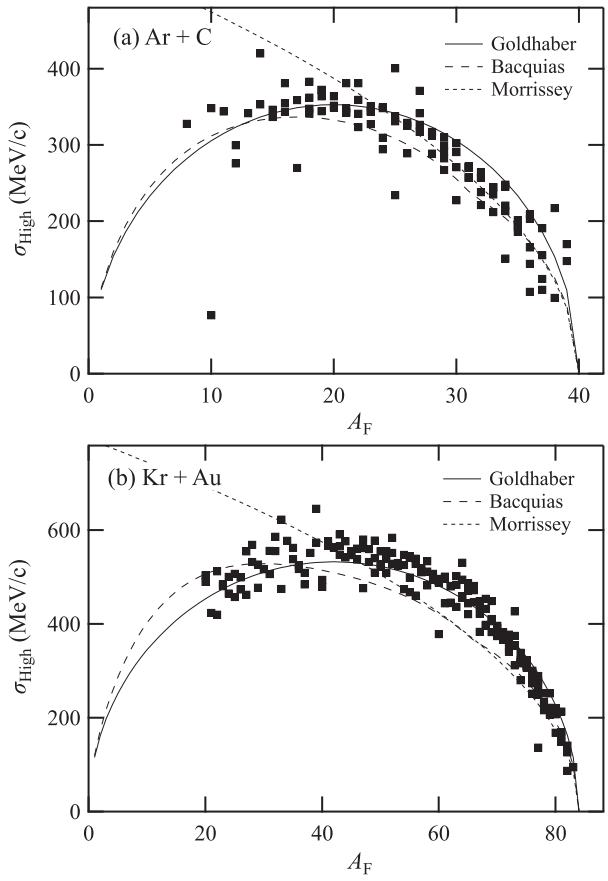

FIG. 12. Width of P_L distribution obtained on the high-P_L side compared with model calculations. For simplicity, error bars are omitted.

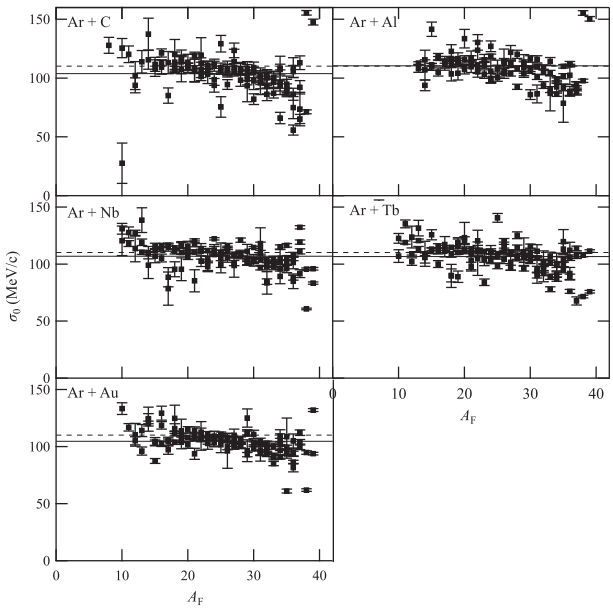

FIG. 13. Reduced width for fragments produced by Ar beam. Solid and broken lines indicate, respectively, the average of observed values for each target and the values obtained by the formulation in Ref. [9].

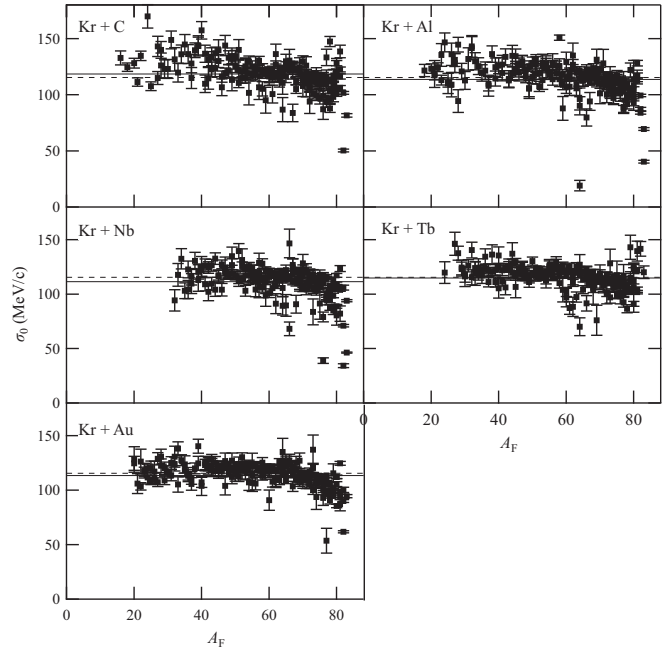

FIG. 14. Reduced width for fragments produced by Kr beam. Solid and broken lines as described in Fig. 13.

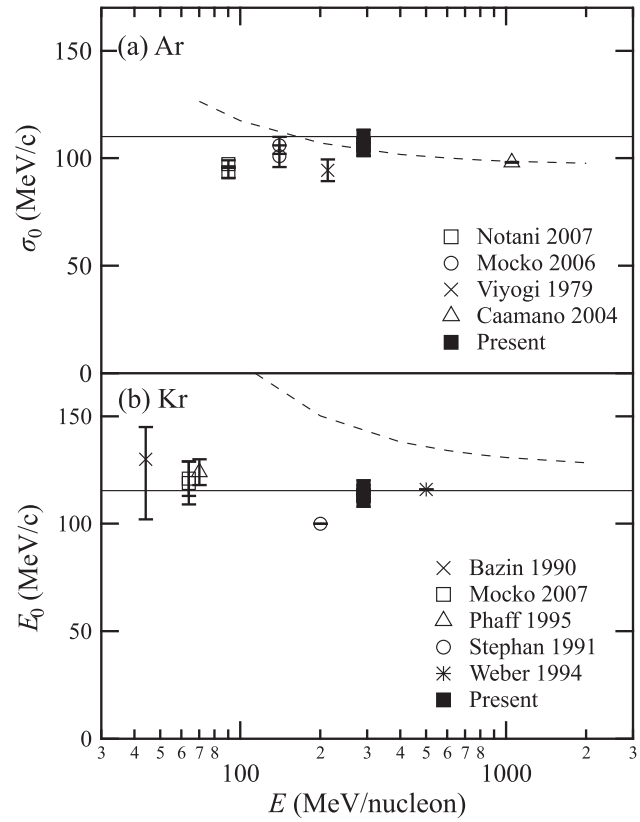

FIG. 15. Energy dependence of reduced width. Solid squares indicate the present results. Other symbols indicate experimental results in Notani [12], Mocko [24], Viyogi [25], and Caamano [26] with Ar beam and those in Bazin [27], Mocko [28], Phaff [8], Stephan [22], and Weber [14] with Kr beam. Solid and broken lines indicate values calculated through the formulas in Refs. [9] and [6].

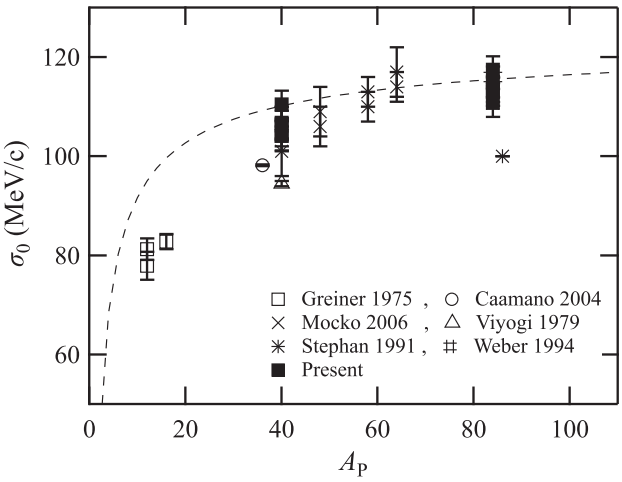

FIG. 16. Reduced width as a function of A_P. Solid squares indicate the present results. Other symbols indicate experimental results in Greiner [3], Caamano [26], Mocko [24], Viyogi [25], Stephan [22], and Weber [14]. Broken lines indicate values calculated by the formulas in Ref. [9].

IV. CONCLUSIONS

P_L distributions of fragments produced by ^{40}Ar and ^{84}Kr beams with targets having a wide range of A_F were systematically investigated at $E = 290$ MeV/nucleon. The momentum peak shift (ΔP_L) and width (σ_{High} and σ_{Low}), which characterize the P_L distribution, were successfully obtained from the observed P_L distributions. No significant target dependence was identified. σ_{High} was successfully reproduced by the Goldhaber formula. In addition, the behavior of σ_0, which was determined from σ_{High}, is consistently explained based on the mass-dependent Fermi momentum, p_F. These results validate the participant-spectator model at this energy, especially on the high-P_L side. On the other hand, σ_{Low}, which is larger than σ_{High}, indicated the contribution of additional reaction processes on the low-P_L side. Theoretical studies are required to elucidate the reaction mechanism on the low-P_L side. The systematics of ΔP_L, σ_{High}, and σ_{Low} were analyzed and represented by a set of formulas. The present findings are useful for assessing the production and transportation of fragments at radioactive nuclear beam facilities.

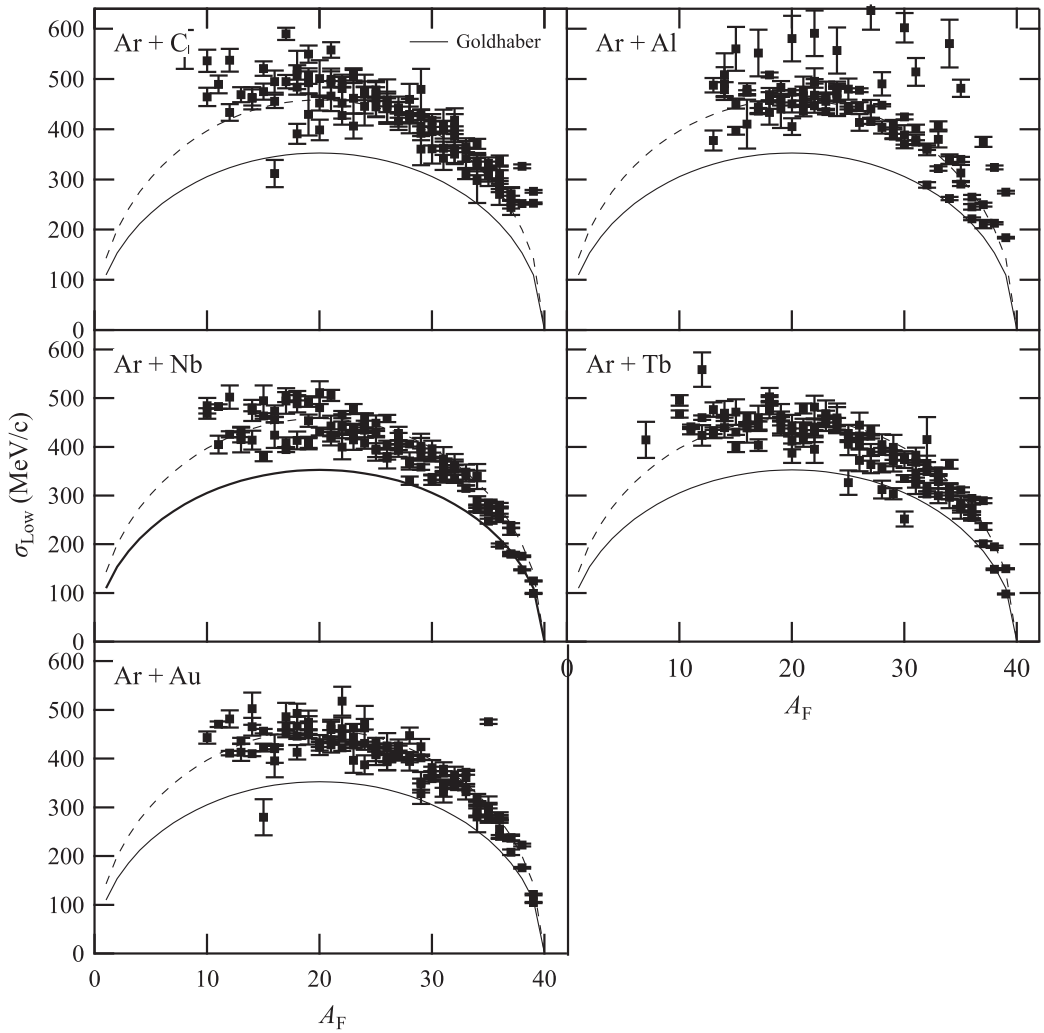

FIG. 17. Width of P_L distribution obtained on the low-P_L side for Ar beam. Solid lines as described in Fig. 10. Broken lines indicate values 30% larger than the solid lines.

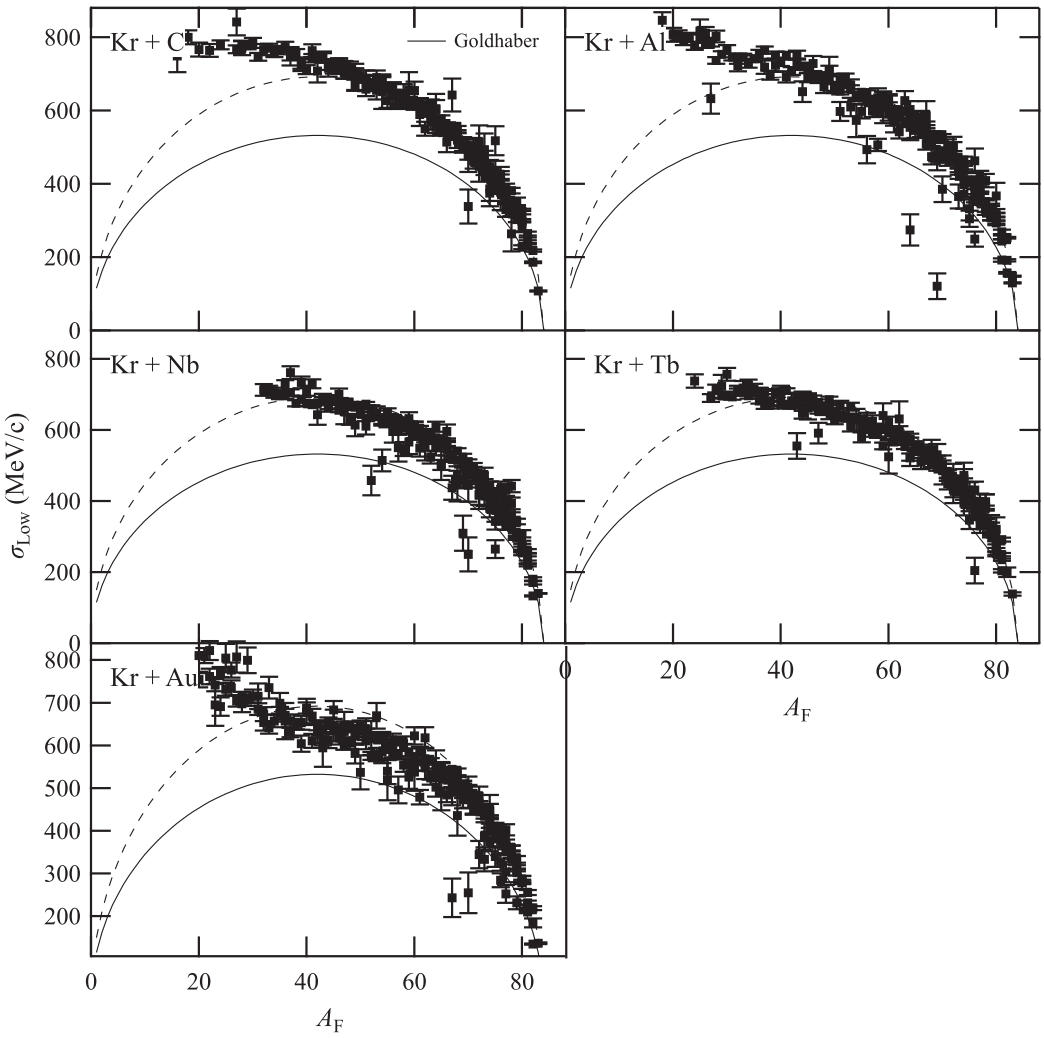

FIG. 18. Width of P_L distribution obtained on the low-P_L side for Kr beam. Solid and broken lines as in Fig. 17.

ACKNOWLEDGMENTS

These experiments were supported by the Research Project with Heavy Ions at the HIMAC accelerator facility of NIRS.

[1] O. B. Tarasov and D. Bazin, Nucl. Instr. and Meth. B **266**, 4657 (2008).
[2] N. Iwasa, H. Geissel, G. Münzenberg, C. Scheidenberger, Th. Schwab, and H. Wollnik, Nucl. Instr. Meth. B **126**, 284 (1997).
[3] D. E. Greiner, P. J. Lindstrom, H. H. Heckman, B. Cork, and F. S. Bieser, Phys. Rev. Lett. **35**, 152 (1975).
[4] A. S. Goldhaber, Phys. Lett. B **53**, 306 (1974).
[5] D. J. Morrissey, Phys. Rev. C **39**, 460 (1989).
[6] R. K. Tripathi and L. W. Townsend, Phys. Rev. C **49**, 2237 (1994).
[7] W. A. Friedman, Phys. Rev. C **27**, 569 (1983).
[8] R. Pfaff, D. J. Morrissey, M. Fauerbach, M. Hellstrom, J. H. Kelley, R. A. Kryger, B. M. Sherrill, M. Steiner, J. S. Winfield, J. A. Winger, S. J. Yennello, and B. M. Young, Phys. Rev. C **51**, 1348 (1995).
[9] M. Giacomelli, L. Sihver, J. Skvarč, N. Yasuda, and R. Ilić, Phys. Rev. C **69**, 064601 (2004).
[10] F. Rami, J. P. Coffin, G. Guillaume, B. Heusch, P. Wagner, A. Fahli, and P. Fintz, Nucl. Phys. A **444**, 325 (1985).
[11] V. Borrel, D. Guerreau, J. Galin, B. Gatty, D. Jacquet, and X. Tarrago, Z. Phys. A **314**, 191 (1983).
[12] M. Notani, H. Sakurai, N. Aoi, H. Iwasaki, N. Fukuda, Z. Liu, K. Yoneda, H. Ogawa, T. Teranishi, T. Nakamura, H. Okuno, A. Yoshida, Y. X. Watanabe, S. Momota, N. Inabe, T. Kubo, S. Ito, A. Ozawa, T. Suzuki, I. Tanihata, and M. Ishihara, Phys. Rev. C **76**, 044605 (2007).
[13] S. B. Kaufman, M. S. Freedman, D. J. Henderson, E. P. Steinberg, B. D. Wilkins, A. Baden, H. H. Gutbrod, M. R. Maier, J. Peter, H. G. Ritter, H. Stelzer, A. I. Warwick, H. H. Wieman, and F. Weik, Phys. Rev. C **26**, 2694 (1982).
[14] M. Weber, C. Donzaud, J. P. Dufour, H. Geissel, A. Grewe, D. Guillemaud-Mueller, H. Keller, M. Lewitowicz, A. Magel, A. C. Mueller, G. Münzenberg, F. Nickel, M. Pfützner, A. Piechaczek,

M. Pravikoff, E. Roeckl, K. Rykaczewski, M. G. Saint-Laurent, I. Schall, C. Stéphan, K. Sümmerer, L. Tassan-Got, D. J. Vieira, and B. Voss, Nucl. Phys. A **578**, 659 (1994).

[15] S. Momota, M. Kanazawa, A. Kitagawa, and S. Sato, J. Korean Phys. Soc. **59**, 1868 (2011).

[16] H. Geissel, C. Scheidenberger, P. Malzacher, J. Kunzendorf, and H. Weick, computer code ATIMA, GSI, https://web-docs.gsi.de/~weick/atima/.

[17] M. Kanazawa, A. Kitagawa, S. Kouda, T. Nishio, M. Torikoshi, K. Noda, T. Murakami, S. Sato, M. Suda, T. Tomitani, T. Kanai, Y. Futami, M. Shinbo, E. Urakabe, and Y. Iseki, Nucl. Phys. A **746**, 393c (2004).

[18] S. Momota, M. Kanazawa, A. Kitagawa, and S. Sato, Nucl. Phys. A **958**, 219 (2017).

[19] C. Scheidenberger, Th. Stöhlker, W. E. Meyerhof, H. Geissel, P. H. Mokler, and B. Blank, Nucl. Instr. Meth. B **142**, 441 (1998).

[20] K. Van Bibber, D. L. Hendrie, D. K. Scott, H. H. Weiman, L. S. Schroeder, J. V. Geaga, S. A. Cessin, R. Treuhaft, Y. J. Grossiord, J. O. Rasmussen, and C. Y. Wong, Phys. Rev. Lett. **43**, 840 (1979).

[21] M. Mocko, Ph.D. Thesis, Michigan State University, 2006.

[22] C. Stéphan, L. Tassan-Got, D. Bachelier, C. O. Bacri, R. Rimbot, B. Borderie, J. L. Boyard, F. Clapier, C. Donzaud, T. Hennino, M. F. Rivet, P. Roussel, D. Bazin, C. Grunberg, D. Disdier, and B. Lott, Phys. Lett. B **262**, 6 (1991).

[23] A. Bacquias, V. Föhr, D. Henzlova, A. Kelic-Heil, M. V. Ricciardi, and K.-H. Schmidt, Phys. Rev. C **85**, 024904 (2012).

[24] M. Mocko, M. B. Tsang, L. Andronenko, M. Andronenko, F. Delaunay, M. Famiano, T. Ginter, V. Henzl, D. Henzlová, H. Hua, S. Lukyanov, W. G. Lynch, A. M. Rogers, M. Steiner, A. Stolz, O. Tarasov, M.-J. van Goethem, G. Verde, W. S. Wallace, and A. Zalessov, Phys. Rev. C **74**, 054612 (2006).

[25] Y. P. Viyogi, T. J. M. Symons, P. Doll, D. E. Greiner, H. H. Heckman, D. L. Hendrie, P. J. Lindstrom, J. Mahoney, D. K. Scott, K. Van Bibber, G. D. Westfall, H. Wieman, H. J. Crawford, C. McParland, and C. K. Gelbke, Phys. Rev. Lett. **42**, 33 (1979).

[26] M. Caamano, D.Cortina-Gil, K. Sümmerer, J. Benlliure, E. Casarejos, H. Geissel, G. Münzenberg, and J. Pereira, Nucl. Phys. A **733**, 187 (2004).

[27] D. Bazin, D. Guerreau, R. Anne, D. Guillemaud-Mueller, A. C. Mueller, and M. G. Saint-Laurent, Nucl. Phys. A **515**, 349 (1990).

[28] M. Mocko, M. B. Tsang, Z. Y. Sun, N. Aoi, J. M. Cook, F. Delaunay, M. A. Famiano, H. Hui, N. Imai, H. Iwasaki, W. G. Lynch, T. Motobayashi, M. Niikura, T. Onishi, A. M. Rogers, H. Sakurai, A. Stolz, H. Suzuki, E. Takeshita, S. Takeuchi, and M. S. Wallace, Phys. Rev. C **76**, 014609 (2007).